Dielectric relaxation and polaronic hopping in Mn-substituted LaSrNiO4 nickelates prepared by mechanical milling method

A. Chouket, V. Optasanu, O. Bidault, A. Cheikhrouhou, W. Cheikhrouhou-Koubaa, M. Khitouni

Dielectric relaxation and polaronic hopping in Mn-substituted $LaSrNiO_4$ nickelates prepared by mechanical milling method

A. Chouket[a], V.Optasanu[b,*], O. Bidault[b], A. Cheikhrouhou[a], W. Cheikhrouhou-Koubaa[a], M. Khitouni[c]

[a]*Laboratoire de Physique des Matériaux, Faculté des Sciences de Sfax, BP 1171, Université de Sfax, 3018 Sfax, Tunisia.*

[b]*LaboratoireInterdisciplinaire Carnot de Bourgogne (ICB), UMR 6303 CNRS - Université de Bourgogne FrancheComté, 9 AV. Alain Savary BP 47870, 21078 Dijon Cedex, France.*

[c]*Laboratoire de ChimieInorganique, Ur-11-Es-73, Faculté des Sciences de Sfax, BP 1171, Université de Sfax, 3018 Sfax, Tunisia.*

[*]*Corresponding author: virgil.optasanu@u-bourgogne.fr, tel.:+33.380.39.91.84*

Abstract

The structures, microstructures and dielectric properties of $LaSrNi_{1-x}Mn_xO_4$ (x=0, 0.1, 0.2, 0.3 and 0.5) ceramics synthetized by mechanical milling followed by heat treatment were studied. One single tetragonal phase was revealed in all compounds. Structural parameters were obtained by Rietveld refinement. The substitution of Ni ions by Mn produces a variation of the lattice parameters but no phase change is observed. The surface morphology and elemental analysis of these samples were respectively investigated by Scanning Electron Microscopy (SEM) and energy dispersive X-ray technique (EDS). Giant dielectric response was observed in these ceramics, and at least two relaxations were found on the curve of the temperature dependence of dielectric constant. An equivalent circuit [R-C][R-CPE] was used to fit the experimental data and provide the activation energy of the thermally activated relaxation. The activation energy values confirm the thermally activated small polaronic hopping contribution to the giant dielectric response.

Keywords

Mechanical milling method; K_2NiF_4-type structure; Rietveld refinement; Dielectric measurements; Equivalent circuit

A. Introduction

The materials having the K_2NiF_4-type structure presents several extremely interesting physical phenomena, such as high-temperature superconductivity in cuprates or spin/charge stripes in nickelates. Last years, many authors have focused on materials characterized by colossal dielectric constant (CDC). Last decades there was a significant interest in developments of materials in order to minimize the microelectronics devices such as dielectric resonators, waveguides, filters, duplexers [1–5]. CDC materials have attracted considerable attention since the discovery of $CaCu_3Ti_4O_{12}$ (CCTO) at the end of 90^s [6,7], which showed an extraordinarily high permittivity of 10^5 at room temperature. Researches were further concentrated on three other types of materials to meet the application requirements: ferroelectric oxides, some transition metal oxides and complex perovskites. Complex perovskites were mainly $AFe_{0.5}B_{0.5}O_3$ type (A = Ba, Sr, Ca; B = Nb, Ta, Sb)[8], $Gd_{0.6}Y_{0.4}BaCo_2O_{5.5}$ [9] and $La_{0.5}Sr_{0.5}Ga_{0.6}Ti_{0.4}O_{3-\delta}$ [10]. Many authors, as Lunkenheimer et al. [11,12], Sinclair et al. [13] and Cohen et al. [14] stated that the seeming giant dielectric constants are due to extrinsic effects. Those effects can be attributed to the Maxwell-Wagner interfacial polarization. Traveling charge carriers produces this space charge or interfacial polarization. The most promising dielectric properties were observed in $Sm_{1.5}Sr_{0.5}NiO_4$ ceramics, where the dielectric constant is about 10^5 at high frequency (5 MHz) while the dielectric loss is about 10^{-1}.

The Nickelates system has good consideration in industry in recent years. This is due to their enormous dielectric properties. These compounds are used worldwide in advanced technology. The observation of unusual and high dielectric loss (tan δ) at room temperature has focused the attention to the possible reasons of this loss. A large effort has been devoted to research the suppression of electrical conductivity induced by Mn-substitution in transition-metal oxides. Li et al. [15] have reported the decrease of bulk conductivity in Mn-doped $CaCu_3Ti_4O_{12}$. Qin et al. [16] have reported that the introduction of Mn ions into $Lu_2Fe_2Fe_{1-x}Mn_xO_7$ can efficiently suppress the electrical conducting leakage. After analyzing the relationship between the electrical resistivity and Mn^{3+} content in $La_{0.7}Ca_{0.3}MnO_3$ thin films, De Teresa et al. [17] found that the polaron binging-energy is proportional to the Mn-O octahedral distortion. Contrary to the invariant Al ion, the valence of Mn oxides is complicated, and it may influence the properties of polaron and of dielectric properties. In this condition, improved dielectric properties of $LaSrNiO_4$ can be expected by Mn substitution. Our paper presents the dielectric properties of $LaSrNi_{1-x}Mn_xO_4$.

There are several preparation methods to obtain the compounds that interest us. In the recent years, the mechanical alloying method has been used for various kinds of materials such as alloys or mixed oxides (ABO_3). Hungria et al. describe mechano-chemical synthesis of Ruddlesden-Popper phases with various perovskite layer thicknesses [18]. They have shown that the synthesis of $Sr_2[Sr_{n-1}Ti_nO_{3n+1}]$ compounds with n going from 1 until 3 by milling high-energy, producing a very significant reduction in the time and temperature of reactions compared to the traditional method of ceramic. The milled samples were annealed at different temperatures up to the formation of the layered perovskites in one single step. The mechanical milling is a very useful method for the powder metallurgy for obtaining nanometric powders. It allows also producing

nanostructured alloys from elementary powders. The mechanical milling is interesting because the fine, nanostructured grains are usually accompanied by very interesting mechanical properties, high resistance and hardness. Moreover, the grains structure plays an important role in the dielectric properties of ceramics because of the high ratio surface of the grains boundary/grain volume. That's why the dielectric study of the compounds obtained by mechanical milling is likely to give different properties than any other elaboration method. At our knowledge, we are the first authors to use the mechanical milling method to elaborate oxides derived from K_2NiF_4perovskites-type. High-energy ball milling [19,20] is a very popular technique due to the low-cost, high efficiency and low temperature synthesis. This method was extensively used for the synthesis of rare-earth permanent magnets and intermetallic compounds [21,22]. Also, the mechanical ball milling technique is one of the important methods in powder metallurgy because of the high flexibility, simple control of process parameters and ability to produce a wide range of materials with fine particles. Moreover, mechanical ball milling technique has also been used to produce commercially important alloys, particularly those having a very high melting point [23] and then causing difficulties in the use of techniques based on fusion. Synthesis of these materials has been extensively studied using different synthetic routes, but the mechano-chemical method itself (not as activation) is not yet a common one [24]. Mechano-chemistry is a relatively simple process that uses high-energy ball mills and allows the processing of nanostructured mixed oxides [25]. The mechanical energy given by impact and shear forces during the high frequency movement is transferred to the powder inducing solid state chemical reactions. One of the most important advantages of mechano-chemistry is its capability to produce large material quantities at room temperature and in a very short time.

Ball milling is used in the synthesis described here (resulting in well mixed, homogenous materials with small grain sizes) followed by high temperatures sintering under air to obtain the desired phase and homogeneity. This step leads to larger grain sizes and higher densities compared with samples made exclusively by mechano-chemical routes. Previously, we worked on dielectric and microstructure characterization on $LaSrNiO_4$ ceramics obtained by high-energy mechanical milling method [26]. We revealed a good dielectric constant $\sim 10^5$ at room temperature but a mediocre dielectric loss showing that for potential applications this compound has to be modified in order to optimize its properties. The substitution in nickelates either in the A and B site has strong effects on the physical properties of the compounds. The substitution by some particular elements can produce a variation of the oxygen stoichiometry. The electrical conductivity depends very strongly on the oxygen stoichiometry since the electric behaviour can go from metallic to semi-conductor when the deviation from stoichiometry increases [27]. In the same time, the structural stress state plays a fundamental role on the dielectric properties. In the case of A_2MO_4 a change in the site M can modify the MO_6 octahedron. A distortion in this octahedron allows a delocalization of hopping on the orbitals and consequently a variation of the dielectric properties.

In a previous work [28] we proceed to the substitution of Ni by Al in $La_{1.6}Sr_{0.4}NiO_4$ compounds elaborated by Pechini method and then generate a remarkable variation of the dielectric properties. However, the measured dielectric losses show that this compounds still need to be optimized. These promising results encouraged us to continue the optimisation of the dielectric properties of this family of compounds by proposing the Mn substitution in order to take advantage of the properties (evoked above) that the Mn could bring to these ceramics. In the present work, we combine the high-energy ball milling method and the Mn substitution to obtain the $LaSrNi_{1-x}Mn_xO_4$ ceramics with good giant dielectric constant and low dielectric loss. In order to deeply understand the origin

of the giant dielectric response and improve the dielectric properties, the Mn-substituted $LaSrNiO_4$ ceramics are studied. Micro-structural characterization on at all the compounds was realized by SEM. X-ray diffractometer was used for phase measurement. Rietveld refinement was used to find the structural parameter. The effect of Mn-substitution on the dielectric properties is investigated by dielectric spectrometry. In order to deeply understand the origin of the dielectric behaviour the modelling of the impedance spectra is proposed. The changes of the dielectric response are discussed with respect to the modification of the composition.

B. Experimental conditions

Ceramic $LaSrNi_{1-x}Mn_xO_4$ powder samples with different Mn content (x = 0, 0.1, 0.2, 0.3 and 0.5) were synthesized by a mechano-chemical method using a planetary ball mill (model Micro-Mill Pulverisette 7, Fritsch) from stoichiometric mixtures of La_2O_3 (Aldrich 99.98%), NiO (Aldrich 99 %), MnO_2 (Aldrich 99 %) and SrO. The last one was obtained from calcinations of $SrCO_3$ (Aldrich 98%) at 1200 °C for 12 h. The possible chemical reaction is given by:

$$\tfrac{1}{2}\, La_2O_3 + SrO + (1\text{-}x)NiO + xMnO_2 \rightarrow LaSrNi_{1-x}Mn_xO_4 \qquad (1)$$

These oxides were mixed with respect to the molar ratio of cations. The powder mixture was mechanically activated using a planetary ball mill. To prevent the heating and sticking of the powder to the container walls and balls, and the powder agglomeration during the process, the milling sequence was selected such as 10 min of milling followed by 5 min of stop period. The experiments were carried out using a hardened steel vial with five steel (diameter 10 mm) balls. The mixture of powders was milled for 10 h and the ball-to-powder ratio and the rotational speed were 5:1 and 600 rpm, respectively. The milled sample was then uniaxially pressed into pellets of 12×5 mm^2 and sintered in air at 1300 °C for 8 h with a heating rate of 10 °C min^{-1} and free cooling.

The phase purity of sample was confirmed by X-ray powder diffraction (PHILIPS diffractometer, X'PERT PRO MPD) using CuK_α($\lambda1$= 1.5405 Å; $\lambda2$= 1.5444 Å) radiation. The XRD patterns were collected in the range of 10–90° with a step size of 0.05°. The structure was analysed by the Rietveld method using the FullProf program, and a pseudo-Voigt profile function with preferred orientation correction [29,30]. The microstructure was studied by scanning electron microscope (SEM) at room temperature and the stoichiometric ratio was detected by energy dispersive X-ray spectroscopy (EDS). The dielectric properties of these ceramics were investigated using a dielectric spectrometer (HP 4284) in a wide range of temperature (80– 450 K) and frequency (1 kHz – 1 MHz) with a heating rate of 1 K min^{-1}. Sputtered platinum was adopted as electrodes.

C. Results and discussions

The results of the X-ray diffraction (XRD) pattern analyses at room temperature of $LaSrNi_{1-x}Mn_xO_4$ ($0 \le x \le 0.5$) compounds are shown in Fig. 1. All our samples have the same K_2NiF_4-type structure. The XRD patterns of all our samples have been indexed in the tetragonal lattice with I4/mmm space group. For the substituted compounds, we can observe that as the Mn content increases the most intense diffraction peak shifts to the low angles (see inset Fig. 1). This result indicates an increase of the unit cell with the Mn content ratio. Fig. 2 shows the Rietveld refined X-ray powder diffraction patterns

registered at room temperature for the $LaSrNi_{0.8}Mn_{0.2}O_4$ samples. The tetragonal I4/mmm model was employed for Rietveld refinement with FullProf program. In this model, La/Sr and O2 atoms are located at 4e (0, 0, z) site, Ni/Mn at 2a (0, 0, 0) and O1 at 4c (0, 0.5, 0) position, respectively. The refinement leads to good agreement between the calculated and experimental XRD profiles, as shown Fig. 2.

Table 1 summarizes the structural parameters obtained by Rietveld analysis of the patterns using FullProf program. Fig. 3 shows the evolution of the parameters *a* and *c* and the volume of the unit cell for all compounds. The evolution of the cell parameters with the Mn content *x*, shows the presence of a change in behaviour both for *a* and *c*. The unit

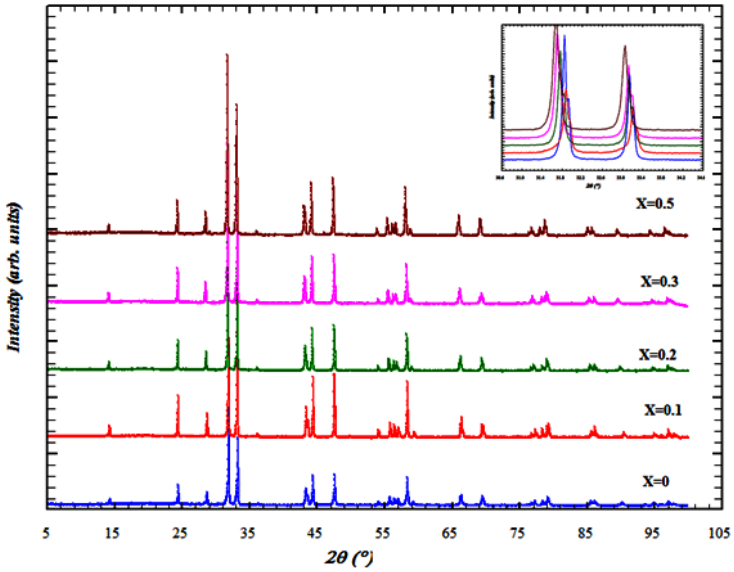

Fig. 1. XRD patterns of $LaSrNi_{1-x}Mn_xO_4$ ceramics sintered at 1300 °C in air for 8h.

cell volume increases with increasing Mn concentration, as illustrated in Table 1. This is due to the effect of the size of the cations occupying site B. On the other hand, the ionic radius of Mn is larger than that of the nickel (r (Ni^{3+}) = 0.56 Å and r (Mn^{3+}) = 0.65 Å). This behaviour can be interpreted from the evolution of the inter-atomic distances listed in Table 2. It is evident that the lengths of La/Sr-O2 (×4) and Ni/Mn-O1 bonds, related to the *a* and *c* parameters, increase with the Mn content. In the same time, the Ni-O2 and La-O2 (×1) bonds that contribute the *c* parameter increase with content of Mn dopants. The decrease in the Ni-O1 and Ni-O2 bond lengths can be explained by the enhanced Jahn-Teller effect caused by the decreasing content of Ni^{3+} [31], while the elongated La-O2 (×1) bonds may result from the electrostatic potential [32]. This result confirms the prevalence of the covalent character of these bonds. Consequently, one can assume that the title compounds have poor ionic features.

Figure 4 shows SEM micrographs of the as-sintered surfaces of $LaSrNi_{1-x}Mn_xO_4$ (x=0, 0.2 and 0.5) ceramics with the same scale. Dense ceramics are obtained, and the grain size decreases with increasing the value of x. The morphology or the grain sizes is not homogeneous in these ceramics. A slight decrease of the grain size is remarked as the Mn content increases. A significant porosity is detected in our compounds. The differences between the microstructures could have an influence on the dielectric properties. We used the SEM backscattered electron mode to identify impurities in the samples. Deductively, no contrast was detected in micrographs, and EDS results shown that the chemical composition of different grains is nearly constant, which confirms the results found by XRD.

The densities of the samples were measured at room temperature with the help of a pycnometer (50ml capacity). The densities were obtained from Archimedes' law. The values of the densities for the compounds x=0, 0.1, 0.2, 0.3, 0.5 were 88.6% (±0.03%), 88.9% (±0.07%), 89.4% (±0.066%), 91% (±0.028%) and respectively 92.6% (±0.02%). The density values are close but a slight increase can however be remarked with the value of Mn content.

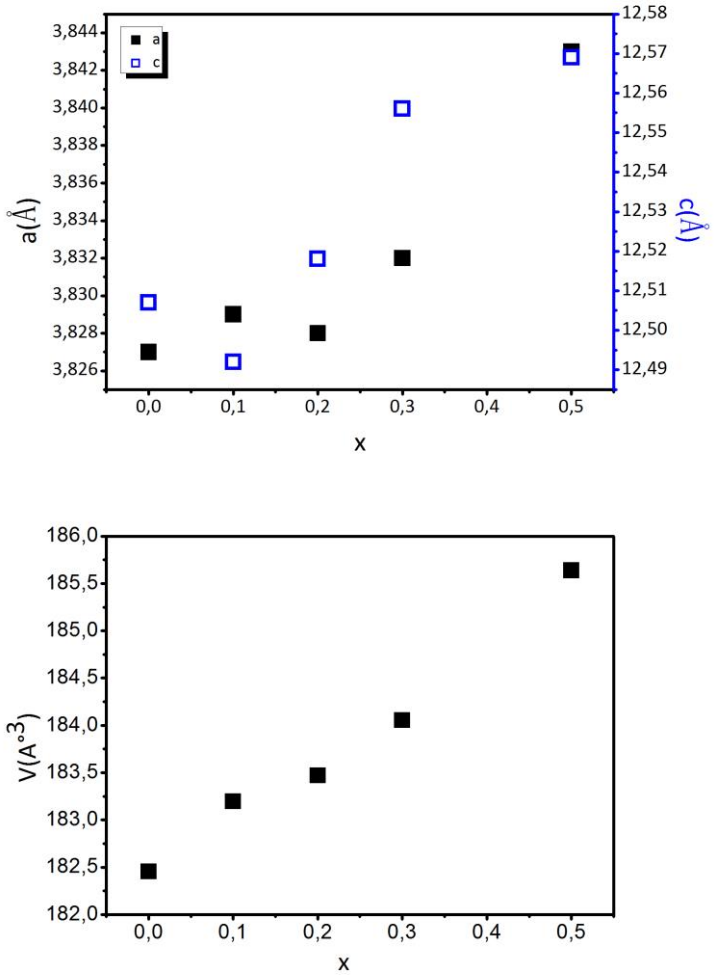

Fig. 3. (a)Lattice parameters *a* and *c*, (b) Unit cell volume *V* of $LaSrNi_{1-x}Mn_xO_4$ obtained from the Rietveld refinements of the XRD measurements.

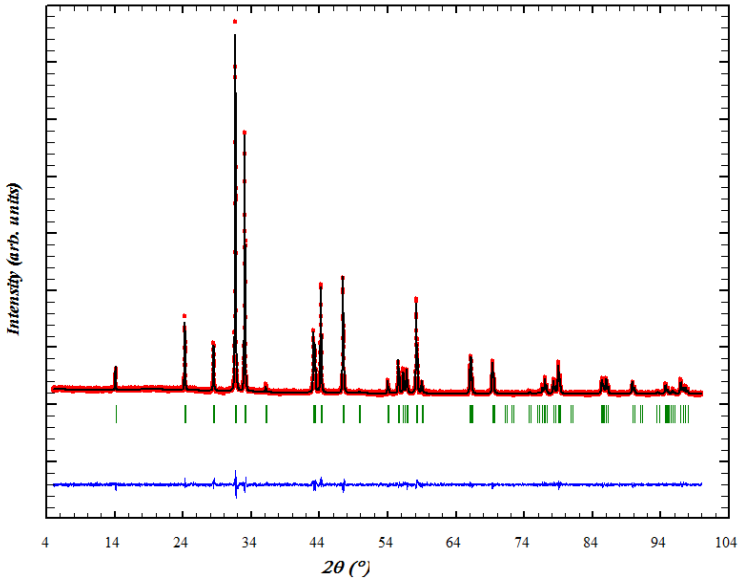

Fig. 2. Rietveld refinement of $LaSrNi_{0.8}Mn_{0.2}O_4$: observed (open circles), calculated (continuous line) and difference (continuous line near the bottom) plots after the final cycle of refinement in the I4/mmm space group. The vertical bars indicate positions of Bragg peaks.

Table.1. Structural parameters of $LaSrNi_{1-x}Mn_xO_4$ ($0 \le x \le 0.50$) resulting from Rietveld refinements of X-ray powder diffraction measurements. Space group is I 4/mmm with La/Sr ions at the 4(e) site with fractional coordinates (0, 0, z), Ni and Mn ions at 2(a) sites with coordinates (0, 0, 0), oxygen O1 at the 4(c) site (0.5, 0, 0) and oxygen O2 at the 4(e) site (0, 0, z). Calculated standard deviations are given in parentheses.

Parameter	x=0	x=0.1	x=0.2	x=0.3	x=0.5
a (Å)	3.8271(4)	3.8290(8)	3.8283(4)	3.8322(6)	3.84304(6)
c (Å)	12.5173(3)	12.4923(2)	12.5185(1)	12.5562(5)	12.5699(4)
Volume (Å³)	182.4552(6)	183.1971(8)	183.4707(2)	184.054 (5)	185.639(3)
La/Sr					
x	0	0	0	0	0
y	0	0	0	0	0
z	0.36093(3)	0.36076 (8)	0.36040(2)	0.36022 (7)	0.35985(9)
Mn/Ni					
x	0	0	0	0	0
y	0	0	0	0	0
z	0	0	0	0	0
O (1)					
x	0	0	0	0	0
y	0.5	0.5	0.5	0.5	0.5
z	0	0	0	0	0
O (2)					
x	0	0	0	0	0
y	0	0	0	0	0
z	0.16429(3)	0.16570(1)	0.16590(3)	0.16657(5)	0.16693(3)
χ2	1.78	1.48	1.65	1.47	1.87

Table.2. Bond lengths of $LaSrNi_{1-x}Mn_xO_4$ for $0 \le x \le 0.50$ as resulting from the Rietveld refinements of the x-ray powder diffraction measurements

Site		x=0	x=0.1	x=0.2	x=0.3	x=0.5
Ni/Mn-O(1) (Å)	x4	1.914(7)	1.915(1)	1.914(2)	1.914(8)	1.922(8)
Ni/Mn-O(2) (Å)	x2	2.046(6)	2.070(3)	2.077(1)	2.077(5)	2.098(5)
La/Sr-O(1) (Å)	x4	2.581(2)	2.587(6)	2.592(4)	2.597(4)	2.607(4)
La/Sr-O(2) (Å)	x1	2.448(4)	2.437(2)	2.435(7)	2.436(4)	2.422(8)
La/Sr-O(2) (Å)	x4	2.725(3)	2.728(8)	2.727(7)	2.726(6)	2.738(2)

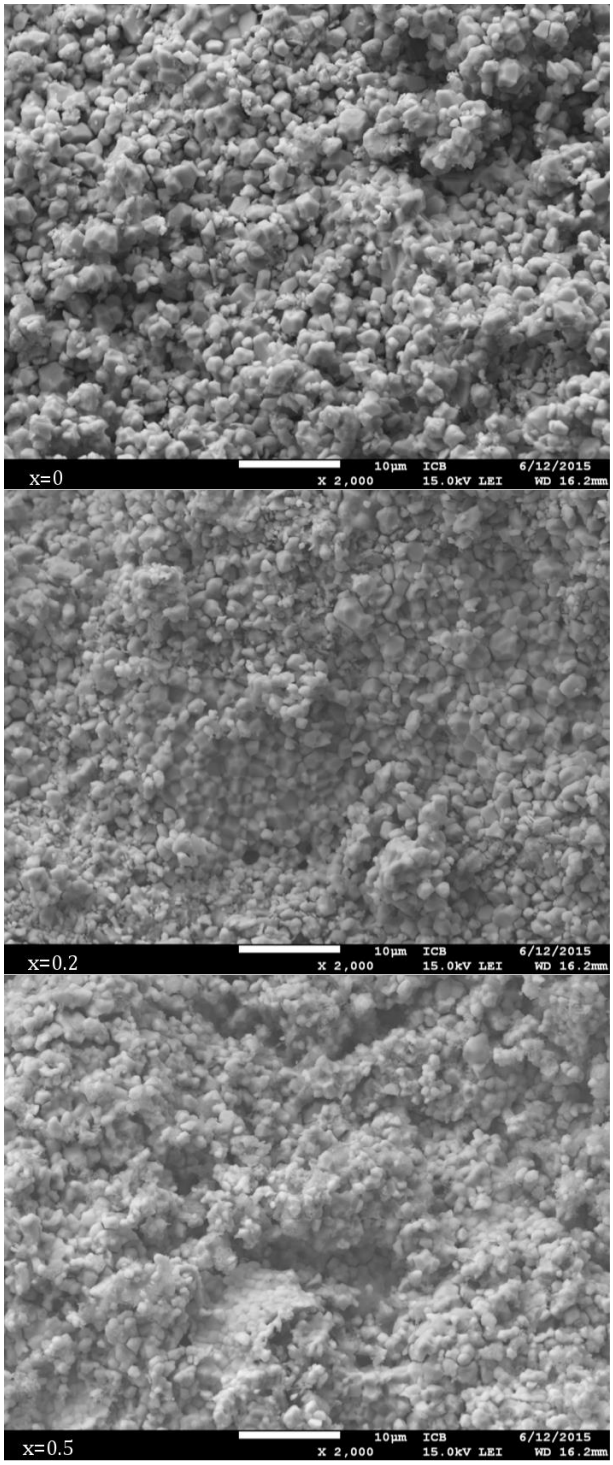

Fig. 4. SEM micrographs of as-sintered surfaces for $LaSrNi_{1-x}Mn_xO_4$ (x=0, 0.2 and 0.5) ceramics. The scale bars represent 10 µm.

Dielectric constant measurements were made in order to study the properties of these compounds. Figure 5 depicts the $\varepsilon^*(\omega)$ spectra recorded at a fixed temperature (293 K) between 1 kHz and 1 MHz for three different samples, namely x = 0 (i.e. without manganese substitution), x = 0.2 and x = 0.5.

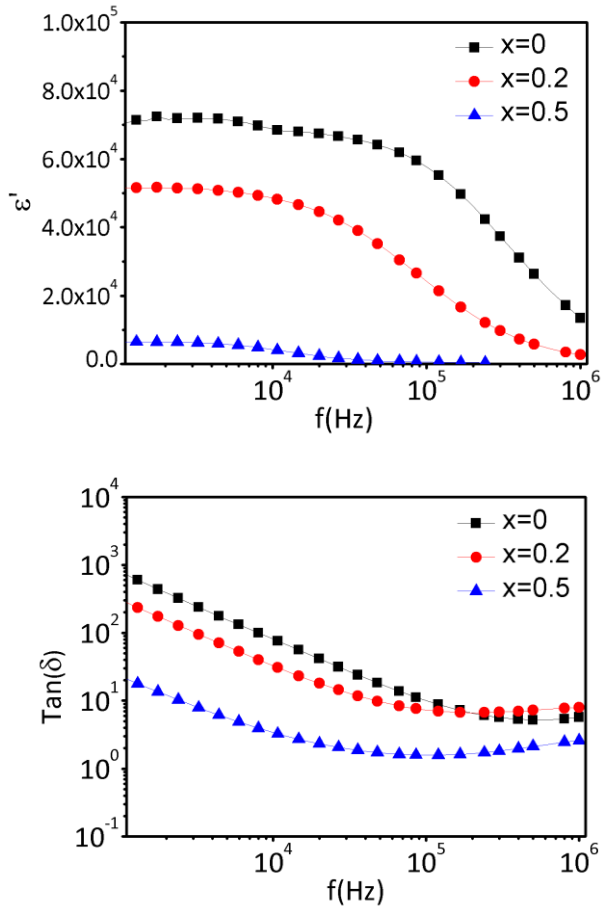

Fig. 5. Dielectric constant of the different $LaSrNi_{1-x}Mn_xO_4$ ceramics (x=0, 0.2, 0.5) recorded as a function of the measuring frequency at room temperature: (a) the real part, ε', and (b) the dielectric losses (ε"/ε').

Looking first at the real part of the dielectric constant, two main features appear: (1) the huge value observed for x = 0 (around 7.10^4 at 1 kHz) gradually decreases as x increases and falls down to about 10^3 for x = 0.5; (2) as the frequency increases, the dielectric constant, that is nearly frequency independent at low frequencies, decreases suddenly down to values of the order of 10^3. The shape of the curve $\varepsilon'(\omega)$ for x = 0 and x = 0.2 is similar to those given by Debye relaxation. One may also note that the relaxation frequency shifts to lower value as x increases. Thus, the huge value of ε' measured at room temperature for x = 0 is coming from a relaxational process. Moreover, this relaxation is highly sensitive to the manganese substitution: as x increases both its amplitude and its characteristic frequency decreases. When x reaches 0.5, the relaxation is no more detectable. We can now look at the losses. For all the sample and measuring frequency, the losses are relatively high (>1) especially in the low frequencies region. Using a log-log scale (fig. 5b), a straight line appears between 1 and 100 kHz, which reflects a $\varepsilon'' \approx \omega^{-1}$

behaviour (because ε' is nearly constant),. This simply means that the losses are mainly dominated by the conductivity; the relaxation is not evidenced by these curves. Here also the manganese significantly changes the losses: as x increases from 0 to 0.5 the conductivity is divided by about hundred.

The conclusion is that the dielectric constant of the highly conductive $LaSrNiO_4$ ceramic is mainly coming from a relaxation; when x increases, the relaxation amplitude and the conductivity are significantly diminished. As half of the Ni cations are replaced by Mn cations, both of them are divided by a factor of about hundred. In order to get more insights on the manganese influence, we have to study the changes induced by a temperature variation.

In figure 6, the real part of the dielectric constant and the losses are reported as a function of the temperature between 100 and 450 K. Three different behaviours, depending on x, can be distinguished:

(1) x = 0 and 0.2: at 1 kHz, the real part of the dielectric constant is nearly temperature-independent, at least for T > 150 K. When the frequency increases, dispersion appears, evidencing a relaxation. This assertion is clear when we look at the ε'(T) curve recorded at 300 kHz, for example, for x = 0.2. When the temperature increases, ε' increases also from 10^3 up to about 10^5. In the same time, the losses, that are quite insensitive to the conductivity at such a high frequency, display a peak near 130 K. This peak shifts to a higher temperature when the frequency increases (about 170 K at 1 MHz) reflecting a thermally activated process (the roughly deduced activation energy is about 55 meV). At lower frequencies, the peak would appear below 100 K. Concerning the losses, they are as high as the measuring frequency is small reflecting the conductivity influence. For x = 0 and 0.2, one thus observes a high conductivity (about 5 $\Omega^{-1}.m^{-1}$ at 300 K and 1 kHz) and a "giant" and single relaxation ($\Delta\varepsilon \approx 10^5$) that we will call hereafter relaxation A.

(2) x = 0.5: the dielectric constant is much smaller (20 - 4000) and has a different behaviour exhibiting a "relaxor-like" shape with a maximum that was not observed earlier. This maximum shifts to a higher temperature as the measuring frequency increases. In the same time, the losses evidence a peak whose position is frequency dependent (from 110 K for 3 kHz to 180 K for 1 MHz implying an activation energy of about 110 meV). However, there is no indication that the sample is a real relaxor; the shape of the ε' curve simply indicates that a relaxation exists in the 100-200 K temperature region. This relaxation (called hereafter B) is different from those observed for x = 0 and 0.2: it has higher activation energy (nearly twice that previously calculated) and much lower amplitude that seems to decreases when the temperature increases. This last point counts for the fact that the dielectric constant shows no more plateau in the high temperature region.

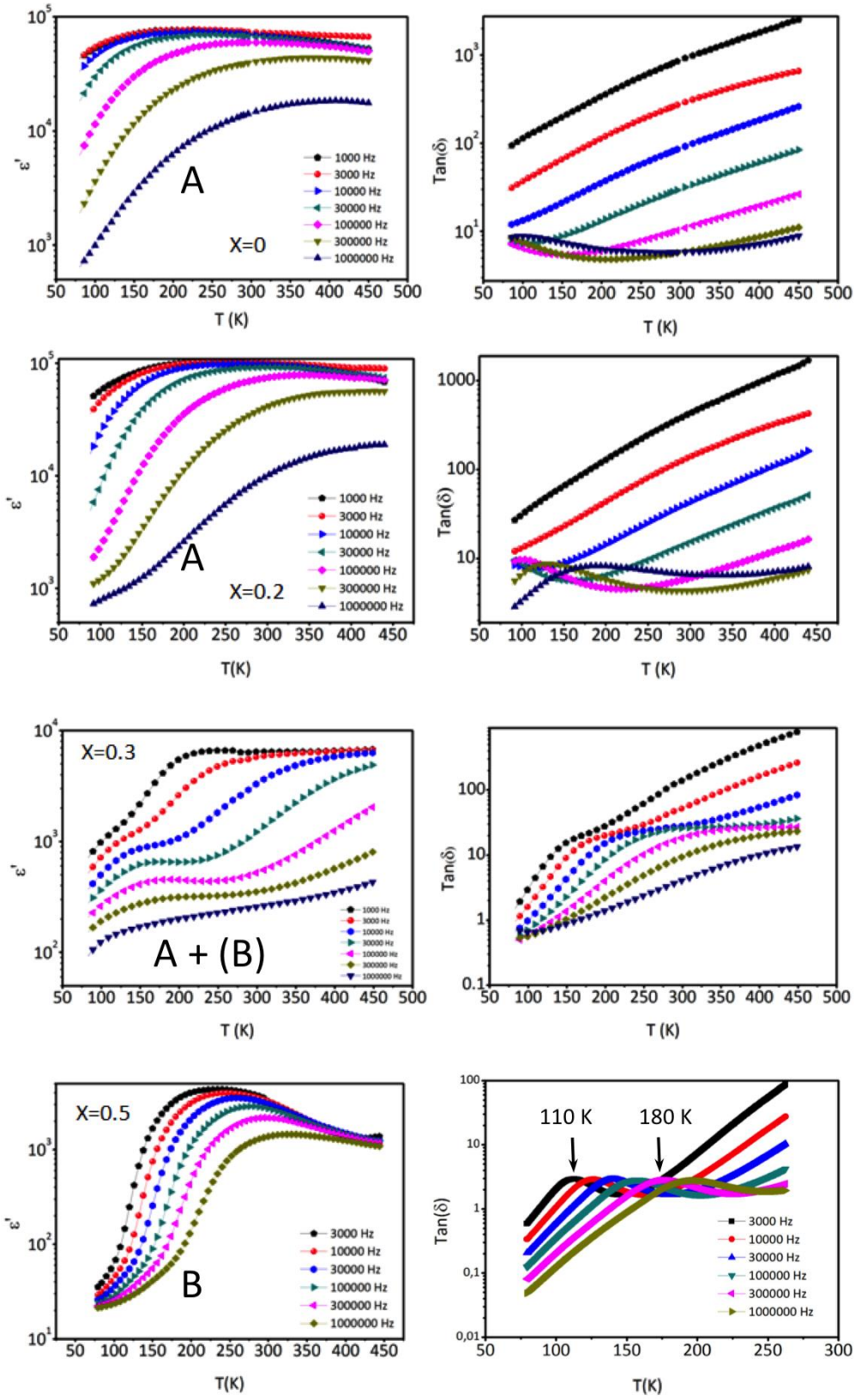

Fig. 6. Temperature dependence (100-450 K) of the dielectric properties (left: ε', right: losses) of the $LaSrNi_{1-x}Mn_xO_4$ ceramics at different fixed frequencies; from high to low: x = 0, x = 0.2, x = 0.3 and x = 0.5. Two different relaxations appear (process A and process B).

(3) x = 0.3 appears as an intermediate case with a rather complex behaviour. In this sample, the two relaxations A and B can be detected inducing still a relatively high and temperature independent dielectric constant at high temperatures ($\varepsilon' \approx 10^4$ for T > 200 K and 1 kHz). When the temperature increases, for example when the frequency is equal to 10 kHz, ε' increases from 300 up to 800 between 100 and 150 K - Process B - followed by a second increase up to 7000 between 250 and 450 K.

From Fig. 6 we may conclude that at least two relaxations exist in the $LaSrNi_{1-x}Mn_xO_4$ system. Both of them are Mn sensitive: when x increases, they shift to a higher temperature and their amplitude decreases. The two extreme cases can be understood as follows: for x = 0, only the process A is detected either because its amplitude is much higher than the one of the relaxation B or, most probably, because the process B occurs at a temperature lower than 100 K. For x = 0.5, the relaxation A is no more detectable allowing the appearance of the weak B process. It is possible to get more informations by analysing the ε(ω) spectra recorded at different temperatures (Fig. 7).

To analyse this dielectric relaxations, the frequency dependence of the dielectric constants for all the ceramics are fitted by the poly-dispersive Cole & Cole equation:

$$\varepsilon^*(\omega) = \varepsilon' - i\varepsilon'' = \varepsilon_\infty + \frac{\varepsilon_s - \varepsilon_\infty}{1+(i\omega\tau)^{1-\alpha}} \qquad (2)$$

Where ε_s is the static dielectric constant, ε_∞ is the dielectric constant at very high frequencies, ω is the angular frequency, τ is the mean relaxation time and α represents the degree of the distribution of the relaxation times τ (α is allowed to change between 0 – i.e. a Debye behaviour with a single relaxation time - to 1).

The fitting results are presented as solid lines in the left part of Fig. 7. The right part of Fig. 7 shows the dependences of the relaxation time on the reciprocal temperatures, and one can find that they obey the Arrhenius law,

$$\tau = \tau_0 \exp\left(\frac{E_a}{k_B T}\right) \qquad (3)$$

where E_a is the activation energy and τ_0 the relaxation time at very high temperatures. The deduced parameters are brought together in table 3.

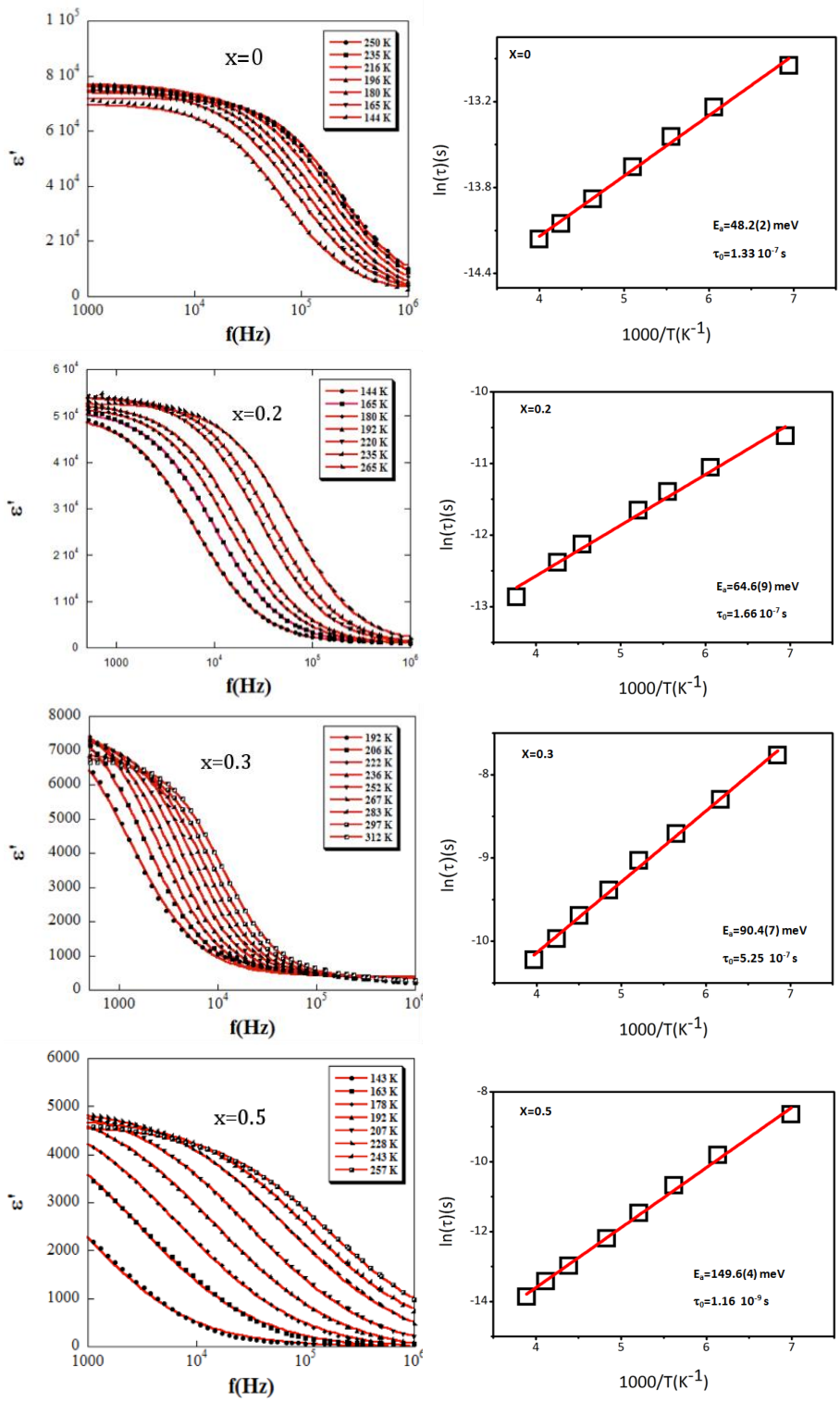

Fig. 7. Real part of the dielectric constant as a function of the frequency recorded at different selected temperatures for x = 0, 0.2, 0.3 and x = 0.5. The studied temperature region changes a little from one sample to another so that we study the process A (140 - 260 K for x = 0 and 0.2 and 190 - 310 K for x = 0.3) or the process B (140 - 260 K for x = 0.5). The points are experimental data and the lines the result of a fit using Eq (2). The deduced relaxation times (squares) are also displayed for each sample in the right part of the figure together with an Arrhenius fit.

Table 3. Fitted parameters that characterize the two relaxations observed in the different samples. They are obtained using Eq. (2) and (3).

Sample	$\Delta\varepsilon = \varepsilon_s - \varepsilon_s$	α	τ_0 (s)	E_a *(meV)*	Relaxation
x = 0	$(7.6 \pm 0.4).10^4$	$\approx 0.35 \pm 0.05$	$\approx 10^{-7}$	48	A
x = 0.2	$(5.0 \pm 0.4).10^4$	$\approx 0.36 \pm 0.02$	$\approx 10^{-7}$	65	A
x = 0.3	7000 ± 300	$\approx 0.45 \pm 0.05$	$\approx 5.10^{-7}$	90	A (+ B)
x = 0.5	$\approx 3222 \exp(\frac{E_{\Delta\varepsilon}}{k_B T})$ $E_{\Delta\varepsilon} \approx 9$ meV	$\approx 0.60 \pm 0.02$	$\approx 10^{-9}$	150	B

If we exclude the most intricate case (x = 0.3), we observe that the process A is slightly polydispersive, characterized by $\tau_0 \approx 10^{-7}$ s and E_a = 50-70 *meV;* moreover, its high amplitude is temperature insensitive. On the contrary, the relaxation B is much polydispersive, has the lowest τ_0 value and the temperature-dependent amplitude follows:

$$\Delta\varepsilon = \Delta\varepsilon_0 \exp(\frac{E_{\Delta\varepsilon}}{k_B T}) \qquad (4)$$

The giant dielectric permittivity observed in some oxides is often suggested to come from electrically heterogeneous regions: in this case, the ceramic consists of semiconducting grains and insulating grain boundaries [33]. This model (called the Maxwell-Wagner effect) was - for example - used to explain the high value of ε' observed in iron based perovskites [8]. The presence of thin and insulating grain boundaries (GB) between grains displaying "intrinsic" or bulk properties is supposed to induce the high permittivity value. Interestingly, in $CaCu_3Ti_4O_{12}$ it was shown that substituting Cu by Mn (even at a low level of about 2%) suppress the bulk semiconductivity and, hence, the enhancement of the dielectric constant [15]. Considering two slabs of different thicknesses, permittivities and conductivities (slab 1: d_{grain}, ε_{grain}, σ_{grain} and slab 2: $d_{GB} << d_{grain}$, $\varepsilon_{GB} \approx \varepsilon_{grain} \approx \varepsilon$ and $\sigma_{GB} << \sigma_{grain}$), the dielectric constant measured at a low frequency is no more the "intrinsic" ε value but a much higher value: $\varepsilon_{measured} = \varepsilon + \Delta\varepsilon \approx \Delta\varepsilon \approx \varepsilon \times d_{grain} / d_{GB}$. In the same time, $\varepsilon(\omega)$ should exhibit a Debye-like relaxation with a relaxation time $\tau = (d_{grain}.\varepsilon) / (d_{GB}.\sigma_{grain})$. This implies that (1) the dielectric constant enhancement (or the relaxation amplitude) is expected to be temperature independent as earlier noticed in table 3 and reported below in Fig. 9 and (2) the activation energy E_a defined in Eq (3) is equal to the activation energy of the bulk conductivity.

To find the relationship between the dielectric relaxation (Process A) and electrical conduction / heterogeneities, the bulk and grain boundary resistances should be found first. Iguchi [34] shows that the impedance spectrum can be used to determine the contribution from the grain volume, grain boundary, and electrode/sample interface. The resistance values of the circuit elements can be obtained from the real axis intercepts. The typical impedance spectra for $LaSrNi_{1-x}Mn_xO_4$ (x=0, 0.2 and 0.5) ceramics at various temperatures were simulated with the EIS Spectrum Analyser software [35] using a [R-C][R-CPE] circuit. The same model was applied for all the samples: it allows to fit the two relaxations whatever their physical origin. In a first time, we will restrict our purpose to x = 0 and x = 0.2. In that case, the [R-C] element account for the grain boundaries and the [R-CPE] circuit corresponds to the bulk. The experimental and simulated results and are shown Fig. 8. At low temperatures 110–250 K, the impedance complex plane plots show

two arcs. Finally, for T > 250K only one arc appears and it does not intercept the origin. The arc produced at high frequency can be attributed to the grain volume while the intermediate frequency arc is due to the grain boundary. In our case, the response of the electrode/sample interface should be out of the frequency range. Using two connected arcs, the least-mean-square analyses are performed and the results are shown as solid lines in the plots (Fig. 8). The right intercept of the high-frequency arc is the resistance of the bulk, while that of the intermediate frequency arc is the total resistances of the bulk and grain boundary. The resistances of the grain/bulk and grain boundary of the present ceramics at different temperatures are obtained from the above analyses, and the values are shown as symbols in right part of Fig. 8. Then the adiabatic small polaronic hopping model can used to fit the extracted data [36-38]:

$$R = R_0 T^{\alpha} \exp\left(\frac{E_{bulk/GB}}{k_B T}\right) \qquad (5)$$

where R_0 is a constant related to the polaron concentration and diffusion, $E_{bulk/GB}$ is the polaronic hopping energy and $\alpha = 1$ for the adiabatic case. The linear relationship between the natural logarithms of R/T value and the reciprocal of temperature is observed in the temperature range of 140–320 K. According to Eq. (5), the activation energies of grain boundaries and bulks are calculated: for x = 0, E_{bulk} = (52 ± 5) meV and E_{GB} = (54 ± 4) meV; for x = 0.2, E_{bulk} = (66 ± 7) meV and E_{GB} = (71 ± 3) meV. In accordance with the Maxwell-Wagner model, the E_{bulk} value is nearly equal to that of dielectric relaxation E_a mentioned above (Table 3). These results show the correlation between dielectric relaxation and the conductivity.

If we now turn to the process B, ie to the relaxation whose amplitude $\Delta\varepsilon$ increases on cooling and which is clearly observed only for x = 0.5, another model should be introduced. This is not the first time that two different relaxational processes are observed in nickelates. For example, the $(Sm_{1-x}Nd_x)_{1.5}Sr_{0.5}NiO_4$ system [39] exhibits an extrinsic Maxwell-Wagner above room temperature but also a low temperature dielectric relaxation ascribed to small polaronic hopping. Kang et al. [39] distinguish two types of relaxations: (1) in the first case, $\Delta\varepsilon$ = constant and the activation energy, E_a - defined in Eq (3) - is similar to the activation energy of the conductivity, E_σ, which is also a thermally activated process:

$$\sigma = \sigma_0 \exp(-\frac{E_\sigma}{k_B T}) \qquad (6)$$

This leads to a space charge model, ie a Maxwell-Wagner effect, in which the relaxation is coming from the long-range motions of the entities responsible for the conductivity; they can be of various types, however all of them contribute to the electrical conductivity. (2) To explain the dielectric anomaly that follows Eq (4), a model based on the short-range hopping of polarized entities (vacancies, polarons...) is introduced. In this second case, the motion of the relaxing species is similar to the reorientation of a dipole and induces a dielectric relaxational peak. In the ideal Debye relaxation, the electrical conductivity is supposed to have no practical relationship with the real part of the dielectric constant (i.e. with the relaxation strength $\Delta\varepsilon$): the conducting carriers do not contribute to the dielectric polarization. If we now suppose that some charge carriers are linked with the relaxation, Kang et al. [40] suggest to modify the Debye equation as following:

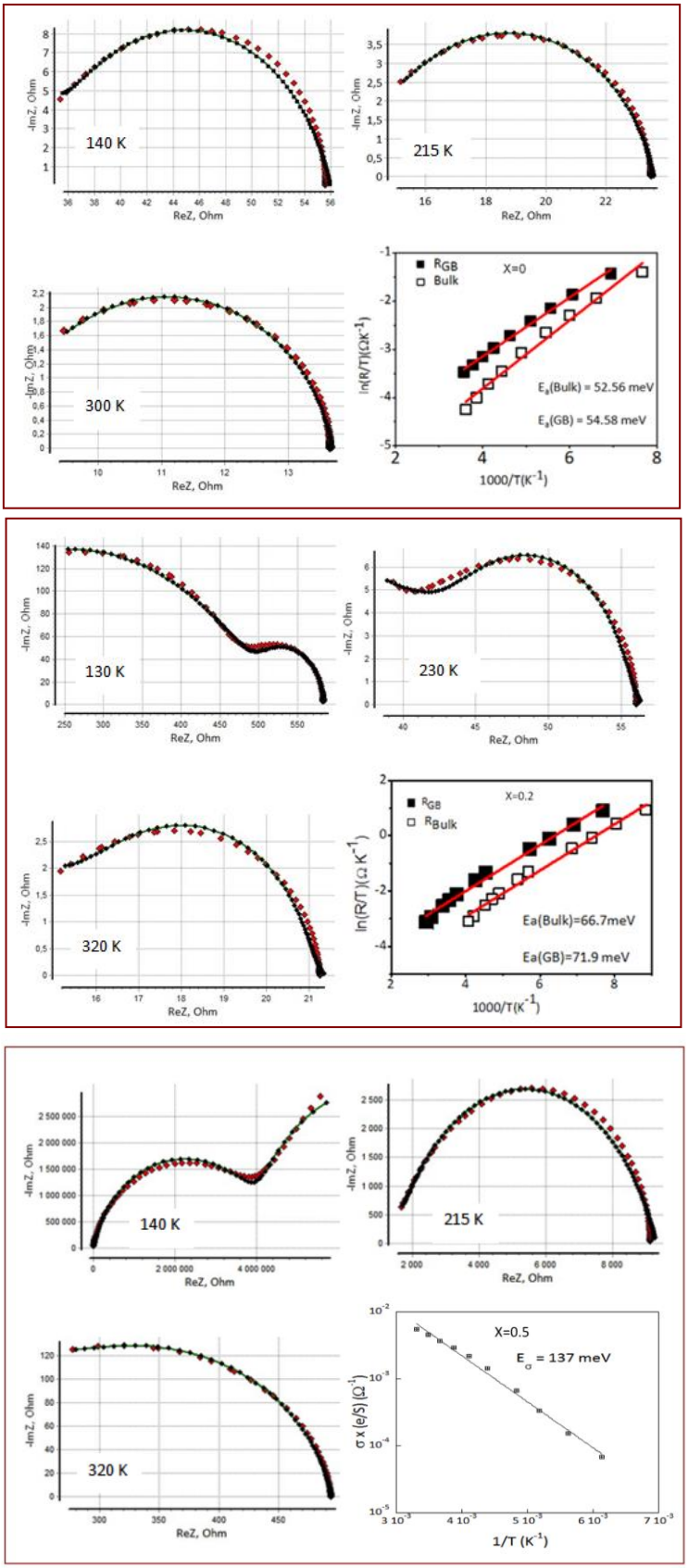

Fig. 8. Complex impedance spectra (dots: measures; solid lines: simulations) of $LaSrNi_{1-x}Mn_xO_4$ ceramics at various temperatures for x= 0, 0.2 and 0.5. Different parameters deduced from the fit (R_{GB}, R_{grain}, the "conductivity" expressed in Ω^{-1}) are reported as a function of 1/T and fitted using Eq (5) for x = 0 and 0.2 or Eq (6) for x = 0.5.

$$\varepsilon' = \varepsilon_\infty + \frac{\Delta\varepsilon.\exp(E_{\Delta\varepsilon}/k_B T)}{1+\omega^2\tau^2} \qquad \text{with } E_{\Delta\varepsilon} = E_a - E_\sigma \qquad (7)$$

This means that the relaxation amplitude is no more constant but thermally activated; the activation energy, $E_{\Delta\varepsilon}$, is then related to the activation energy of both relaxation, E_a, and conductivity, E_σ. All these values have been calculated for x = 0.5. We found E_a = 150 meV (table 2), E_σ = 137 meV (Fig. 8, σ is deduced from the fit of the impedance Z (ω) assuming, instead of Eq (5), a simpler Arrhenius law) and $E_{\Delta\varepsilon}$ = 9 meV (Fig. 9) and note that effectively $E_{\Delta\varepsilon} \approx E_a - E_\sigma$ in accordance with the model.

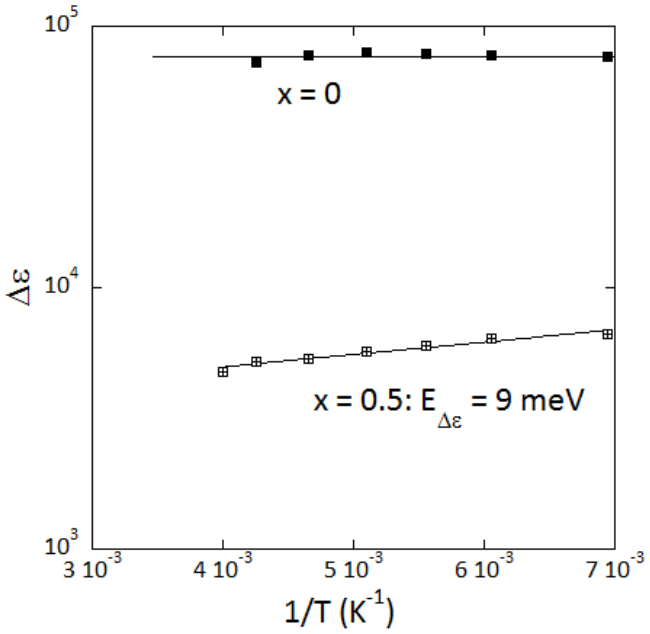

Fig. 9. Relaxation strength Δε deduced from Eq (2) and reported in Table 3 as a function of 1/T for x = 0 and x = 0.5.

D. Conclusions

The main conclusions of this paper can be summarized as follows:

- Bulk $LaSrNi_{1-x}Mn_xO_4$ (x=0, 0.1, 0.2, 0.3 and 0.5) oxides were successfully synthesized by the use of high-energy mechanical milling for 10 h and heat treatment at 1300 °C for 8 h.
- The Rietveld refinement of room temperature XRD patterns on powder indicates one single phase, exhibiting tetragonal structure with space group of I4/mmm and permit to find the lattice parameter.
- Dielectric measurements of the prepared compounds, in the temperature range 80 - 450 K show giant dielectric constants (ε'~10^5) and low dielectric losses (Tan(δ)~1). The very high values of the dielectric constant at room temperature make the material potentially attractive for applications.
- The giant dielectric constant of the $LaSrNi_{1-x}Mn_xO_4$ ceramics is the sum of two distinct contributions: (1) a relaxation occurring between 200 and 300 K and coming from a Maxwell-Wagner effect due to the juxtaposition of conducting and isolating regions, (2) a weaker relaxation (T < 150 K) relating to the short range

motion of some entities that also contribute to the overall conductivity of the samples.

- The poly-dispersion Debye equation was used to fit the ε' - f curves and permits to obtain the activation energy for the relaxation time.
- The simulation of the equivalent circuit impedance, according to the small polaronic model, allowed calculating the activation energy for bulk and grain boundary. The comparison of the activation energy of these two models revealed that the low temperature high-frequency dielectric relaxation of this sample can be attributed to the adiabatic small polaron hopping process.

As a perspective we will consider the influence of the milling time on the dielectric properties of this type of compounds.

References

[1] L. Fang, H. Su, Q. Yu, H. Zhang and B. Wu, *J. Am. Ceram. Soc.,* 2008, **91**, 2769;

[2] X.Q. Liu, B.W. Jia, W. Z. Yang, J.P. Cheng, X.M. Chen, *J. Phys. D: Appl. Phys* 2010, **43**, 495402;

[3] A.K. Jonscher, *Nature* 1977, **9**, 267;

[4] R.D. Shannon, *J. Appl. Phys*. 1993, **73**, 348;

[5] Y. Fink, J.N. Winn, S. Fan, C. Chen, J. Michel, J.D. Joannopoulos, E.L. Thomas, *Science*, 1998, ***282***, 1679;

[6] C. C. Homes, T. Vogt, S. M. Shapiro, S, Wakimoto and A. P. Ramirez, *Science*, 2001, **293**, 673;

[7] P. Lunkenheimer, R. Fichtl, S.G. Ebbinghaus and A. Loidl, *Phys. Rev. B*, 2004, **70**, 172102;

[8] I.P. Raevski, S.A. Prosandeev, A.S. Bogatin, M.A. Malitskaya, L. Jastrabik, *J. Appl. Phys*, 2003, **93**, 4130;

[9] V. Bobnar, P. Lunkenheimer, M. Paraskevopoulos, A. Loidl, *Phys. Rev. B,* 2002, **65**, 184403;

[10] E. Iguchi, S. Mochizuki, *J. Appl. Phys*, 2004, **96**, 3889;

[11] P. Lunkenheimer, V. Bobnar, A. V. Pronin, A. I. Ritus, A. A. Volkov, A. Loidl, *Phys. Rev. B*, 2002, **66**, 052105;

[12] P. Lunkenheimer, R. Fichtl, S. G. Ebbinghaus, A. Loidl, *Phys. Rev. B*, 2004, **70**, 172102;

[13] D.C. Sinclair, T.B. Adams, F.D. Morrison, A.R. West, *Appl. Phys. Lett.*, 2002, **80**, 2153;

[14] M.H. Cohen, J.B. Neaton, L. He, D. Vanderbilt, *J. Appl. Phys.*, 2003, **94**, 3299;

[15] M. Li, A. Feteira, D. C. Sinclair, and A. R. West, *Appl. Phys. Lett.*, 2006, **88**, 232903;

[16] Y.B. Qin, H.X. Yang, Y. Zhang, H.F. Tian, C. Ma, L.J. Zeng, J.Q. Li, *Appl. Phys. Lett.*, 2009, **95**, 072901;

[17] J.M. De Teresa, K. Donn, K.H. Muller, L. Schultz, *Phys. Rev. B*, 1998, **58**, 5928;

[18] T. Hungria, J. G. Lisoni, A. Moure, L. Pardo, A. Castro, *Ferroelectrics,* 2002, **268**, 399;

[19] J. Benjamin, *Sci. Am.*, 1976, **234**, 40;

[20] C. Suryanarayana, *Prog. Mater. Sci.*, 2001, **46**, 1;

[21] Ch. Kuhrt, L. Schultz, *J. Appl. Phys.,* 1992, **71**, 1896;

[22] L. Schultz, K. Schnitzke, J. Wecker, *J. Appl. Phys*., 1988, **64**, 5302;

[23] J. Che, X. Yao, H. Jian, M. Wang, *Ceram. Int*., 2004, **30**, 1935;

[24] M. Wang, K.D. Woo, C.G. Lee, *Energy Conversion and Management* 2011, **52**, 1589;

[25] P. Balaz, M. Achimovicova, M. Balaz, P. Billik, Z. Cherkezova-Zheleva, J. M. Criado, F. Delogu, E. Dutkova, E. Gaffet, F.J. Gotor, R. Kumar, I. Mitov, T. Rojac, M. Senna, A. Streletskii, K. Wieczorek-Ciurowa, *Chem. Soc. Reviews*, 2013, **42**, 7571;

[26] A. Chouket, W. Cheikhrouhou-Koubaa, A. Cheikhrouhou, V. Optasanu, O. Bidault, M. Khitouni, *J. Alloys. Compd,* 2016, **662**, 467;

[27] C. Michel and B. Raveau, Rev. Chim. Min., 1984, 21, 407;

[28] A. Chouket, O. Bidault, V. Optasanu, A. Cheikhrouhou, W. Cheikhrouhou-Koubaa& M. Khitouni, RSC Adv., 2016, **6**, 24543;

[29] H.M. Rietveld, J. Appl. Cryst., 1969, 2, 65;

[30] T. Roisnel, J. Rodriguez-Carvajal, Computer Program FULLPROF, LLB-LCSIM, May 2003;

[31] T. Hotta, *Rep. Prog. Phys.*, 2006, **69**, 2061;

[32] K.K. Singh, P. Ganguly, J.B. Goodenough, *J. Solid State Chem.* 1984, **52**, 254;

[33] P. Lunkenheimer, S. Krohns, S. Riegg, S. G. Ebbinghaus, A. Reller, and A. Loidl, Eur. Phys. J. Special Topics, 2010, **180**, 61;

[34] E. Iguchi, H. Nakatsugawa, and K. Futakuchi, *J. Solid State Chem.*, 1998, **139**, 176;

[35] A. S. Bondarenko, G. A. Ragoisha, *Prog. In Chemometrics Research,* 2005, 89;

[36] X.Q. Liu, S.Y. Wu, X.M. Chen, H.Y. Zhu, *J. Appl. Phys.,* 2008, **104**, 054114;

[37] X.Q. Liu, Y.J. Wu, X.M. Chen, H.Y. Zhu, *J. Appl. Phys.,* 2009, **105**, 054104;

[38] G. Wu, J.J. Neumeier, *Phys. Rev. B,* 2003, **67**, 125116;

[39] B. W. Jia, W. Z. Yang, X. Q. Liu and X. M. Chen, *J. Appl. Phys*, 2012, **112**, 024104;

[40] B. S. Kang, S. K. Choi, C. H. Park, *J. Appl. Phys*, 2003, **94**, 1504.